Did North Atlantic cooling and freshening from 3.65–3.5 Ma precondition Northern Hemisphere ice sheet growth?

Cyrus Karas[1,2,3,4]*, Nabil Khélifi[5,6], André Bahr[7], B.D.A. Naafs[8,9], Dirk Nürnberg[6], Jens O. Herrle[1]

[1]Goethe-University Frankfurt, Altenhoeferallee 1, 60438, Frankfurt am Main, Germany
[2]Lamont Doherty Earth Observatory of Columbia University, Palisades, NY 10964, USA
[3] Instituto de Geografía, Pontificia Universidad Católica de Chile, Santiago, Chile
[4] Millennium Nucleus Paleoclimate, University of Chile, Santiago, Chile
[5] Springer, a part of Springer Nature, Tiergartenstrasse 17, 69121, Heidelberg, Germany
[6] GEOMAR Helmholtz Centre for Ocean Research Kiel, Wischhofstrasse 1-3, 24148 Kiel, Germany
[7] Ruprecht-Karls-Universität Heidelberg, Institut für Geowissenschaften, Im Neuenheimer Feld 234, 69120 Heidelberg, Germany
[8] Organic Geochemistry Unit, School of Chemistry and Cabot Institute, University of Bristol, Bristol, UK
[9] School of Earth Sciences, University of Bristol, Bristol, UK

* Email address of corresponding author: cyrus.karas@uc.cl

Abstract

The North Atlantic Current (NAC) as part of the Atlantic Meridional Overturning Circulation (AMOC) is the major supplier of heat into the northern North Atlantic. Pliocene changes of AMOC strength were speculated to either have amplified or diminished the Northern Hemisphere Glaciation (NHG) 2.7 million years ago (Ma). However, from the North Atlantic, little evidence is known about AMOC changes at around 3.6 Ma. At this time the intensification of NHG started and culminated in the first major glacial M2 event at 3.3 Ma. To elaborate the climatic effects of variations in the NAC during this early stage of NHG, we here present millennial-scale resolved records from Deep Sea Drilling (DSDP) Site 610A in the northern North Atlantic. Our data of planktic foraminiferal Mg/Ca-based sea surface temperatures ($SST_{Mg/Ca}$) and ice volume corrected salinity approximations ($\delta^{18}O_{IVC\text{-}seawater}$) span the critical time period 4-3.3 Ma. From 3.65 to 3.5 Ma, we observe a distinct ~3.5 ºC cooling and ~0.7‰ freshening of the sea surface, which we interpret to reflect a weakened NAC. At the

same time Arctic sea ice grew and benthic $\delta^{13}C$ in the South Atlantic suggest a weakened AMOC. We conclude that the weakened NAC in response to a sluggish AMOC fostered sea ice formation in the Arctic Ocean and high-latitude North Atlantic, which might have preconditioned the climate for subsequent continental glaciations.

Keywords

Pliocene, Northern Hemisphere Glaciation, NAC, AMOC, foraminiferal Mg/Ca,

1. Introduction

Today, the heat transport amounting to 0.6–0.7 PW through the Atlantic Meridional Overturning Circulation (AMOC) sustains relatively mild conditions in the high-latitude North Atlantic and its surrounding land masses (Jackson et al., 2015, Trenberth and Fasullo, 2017). The upper limb of this current system is the heat and salt transport from the Caribbean into the northern North Atlantic via the Gulf Stream and its northward extension, the North Atlantic Current (NAC; Fig. 1a). This warm and saline water transported by the NAC cools on the way towards the north. It remains relatively salty and therefore sinks to depth in the Norwegian Sea and the Labrador Sea to ultimately form North Atlantic Deep Water (NADW), the lower limb of the AMOC (Fig. 1a, b).

The intensity of AMOC/NAC has been dynamic over geological time scales and has been hypothesized to play a major role in the build-up of continental ice-sheets in the Northern Hemisphere at different times during the Pliocene. First, a strengthening of the AMOC in response to the closing of the Central American Seaway (CAS) was proposed for the period 4.8-4.0 Ma (Haug and Tiedemann, 1998; Steph et al., 2010; Karas et al., 2017). This tectonically-induced onset and intensification of the AMOC would have provided atmospheric moisture towards the Northern Hemisphere, preconditioning the climate system for major Northern Hemisphere glaciation (NHG; Haug and Tiedemann, 1998). However,

63 these changes in AMOC occurred at a time of global warmth well before the intensification of
64 Northern Hemisphere Glaciation (iNHG) that took place from ~3.6 to 2.4 Ma (Mudelsee and
65 Raymo, 2005). Further, an increased northward heat transport via the AMOC would also have
66 transported excess heat to the high-latitudes, inhibiting ice sheet growth (Haug and
67 Tiedemann, 1998; Driscol and Haug, 1998; Lunt et a l., 2008).

68 For the critical time around 3.6 Ma, which marks the beginning of the iNHG
69 (Mudelsee and Raymo, 2005), high-resolution SST and salinity reconstructions are still
70 missing from the northern North Atlantic. This hinders a holistic assessment of the past
71 changes in the NAC during this crucial time period and ultimately, understanding the
72 mechanism(s) that drove the iNHG. Published sea surface temperature (SST) and salinity
73 gradients between the North and South Atlantic oceans showed a reduction of AMOC
74 between 3.8-3.0 Ma (Karas et al., 2017). However, around 3.6 Ma, the resolution of the North
75 Atlantic Site 552A record is insufficient to reliably infer changes in the NAC (Karas et al.,
76 2017).

77 To investigate the state of the northward heat transport during the 4.3–3.3 Ma interval,
78 we here reconstruct changes in the surface NAC using a multiproxy approach. We use
79 orbitally-resolved records (resolution of 3-4 kyrs) of Mg/Ca ratios in planktic foraminiferal to
80 obtain $SST_{Mg/Ca}$ and combine these with planktic foraminiferal $\delta^{18}O$ to estimate surface
81 paleosalinities from DSDP Site 610A in the North Atlantic. To infer changes in the deeper
82 AMOC circulation we use published benthic foraminiferal $\delta^{13}C$ records from the South
83 Atlantic (Bell et al., 2014). Site 610A (53°13'N; 18°53'W; see Fig. 1a, b for location) is
84 situated on the Rockall Plateau at 2417 m water depth. In the modern, the NAC flows over
85 Site 610A, making it an ideal candidate to trace changes in the NAC in the past.

86

87 **2. Material and Methods**

88 *2.1 Stable oxygen isotopes, Mg/Ca data, and age model*

For the preparation of foraminifera for $\delta^{18}O$ and Mg/Ca analyses we followed previous studies (Karas et al., 2009; 2017). Before geochemical analyses, all sediments were freeze-dried and subsequently washed over a 63 μm mesh sieve. The residue was dried and fractionated into various size fractions. For the $\delta^{18}O$ and Mg/Ca analyses we used the 215-315 μm size fraction to select ~30 specimens (min. ~12; max. ~40) of near-surface dwelling foraminifera *Globigerinoides bulloides* (approx. depth habitat of upper 50-60 m; Jonkers et al., 2013; Schiebel et al., 1997). The selected foraminiferal tests were optically crushed under a binocular, mixed, and divided into 2/3 for Mg/Ca analyses and 1/3 for $\delta^{18}O$ analyses. $\delta^{18}O$ analyses were conducted on a Thermo Scientific MAT253 equipped with a Gas Bench II (Goethe-University Frankfurt) with an analytical precession (1σ) of ±0.08 ‰.

The foraminiferal fragments for Mg/Ca analyses were cleaned according to an established cleaning protocol (Barker et al., 2003; without reductive step). Analyses of elements were carried using an iCAP 6300 (Thermo Scientific™) ICP-OES at Goethe-University Frankfurt. Yttrium (Y) was used as an internal standard to correct for analytical drift and minimize matrix-effects. Analytical lines were 280.2 nm (Mg) and 315.8 nm (Ca). Mn (257.6 nm) and Fe (238.2 nm) were monitored to infer possible contamination by clay minerals and diagenetic phases. All measurements were done in axial mode. Molar M/Ca ratios (M = trace element) were computed via intensity ratio calibration (de Villiers et al., 2002). Mg/Ca ratios were normalized based on repeated measurements of the ECRM 752-1 carbonate standard using the Mg/Ca ratio of 3.762 mmol/mol (Greaves et al., 2008). Replicate analyses of 5 samples (aliquots of crushed samples) showed a standard deviation of 0.16 mmol/mol for Mg/Ca. There was no contamination through diagenetically Mn crusts nor through terrigenous input indicated by low Mn/Ca and Fe/Ca ratios. Average Mn/Ca ratios were ~0.19 mmol/mol and Fe/Ca ratios were mostly below the detection limit (for Mg/Ca, Mn/Ca and Fe/Ca downcore records see Supplementary figure 1). Only two samples showed exceptionally high Fe/Ca values (both ~1.1 mmol/mol). We decided not to discard these as

115 the corresponding Mg/Ca values showed no abnormal high values (2.76 and 3.16 mmol/mol,
116 respectively).

117 Consistent with previous studies from the North Atlantic (e.g., De Schepper et al.,
118 2013; Karas et al., 2017) we used the multispecies calibration of Elderfield and Ganssen
119 (2000) (Mg/Ca = 0.52 (±0.0085) exp (0.10 x SST)) to convert Mg/Ca ratios into $SST_{Mg/Ca}$. We
120 assumed that the Mg/Ca of seawater was the same during the Pliocene as at modern. The
121 propagated error for the resulting $SST_{Mg/Ca}$ estimates is about ± 0.6 ºC. Calcite dissolution is
122 unlikely to have occurred at Site 610A during the Pliocene as close-by Site 552A, which is
123 from a similar water depth, was found to be unaffected by dissolution processes (indicated by
124 foraminiferal test weights) during the same time period (Karas et al., 2017).

125 The age model used for Site 610A is from Naafs et al. (in revision) and is based on
126 high-resolution (3.5 kyrs) benthic $\delta^{18}O$ stratigraphy tuned to the LR04 benthic $\delta^{18}O$ stack
127 (Lisiecki and Raymo, 2005).

128

129 *2.2 Calculation of $\delta^{18}O_{seawater}$ and $\delta^{18}O_{IVC\text{-}seawater}$*

130 First, $\delta^{18}O_{seawater}$ values were calculated from our *G. bulloides* $SST_{Mg/Ca}$ and $\delta^{18}O$ values after
131 Shackleton (1974): $T= 16.9- 4.38 \times (\delta^{18}O_{foram}- \delta^{18}O_{seawater}) + 0.1 \times (\delta^{18}O_{foram} - \delta^{18}O_{seawater}$; Fig.
132 2a, b). By doing so the initial $\delta^{18}O$ values in the PDB scale were adjusted to the SMOW scale
133 by adding 0.27 ‰ (Hut, 1987). These values are already a good indication for changes in
134 surface salinity as changes in global ice volume are relatively small during the Pliocene
135 compared to the colder Pleistocene glacial-interglacial cycles (Lisiecki and Raymo et al.,
136 2005). However, as global ice volume also slightly increased during 3.6–3.3 Ma, we corrected
137 the initial $\delta^{18}O_{seawater}$ values. Here we used the ice volume record of de Boer et al. (2014) that
138 is expressed as the global ice volume component of marine benthic $\delta^{18}O$ ($\delta^{18}O_{GIV\text{-}seawater}$; Fig.
139 2d). This record was calculated based on the global LR04 stack (Lisiecki and Raymo, 2005)
140 and simulations of continental ice sheets (de Boer et al., 2014). Subtracting this $\delta^{18}O_{GIV\text{-}seawater}$

141 record from our initial $\delta^{18}O_{seawater}$ values yielded the final ice volume corrected $\delta^{18}O_{IVC\text{-}seawater}$
142 record, which we use to approximate changes in Pliocene salinities (Fig. 2c). The propagated
143 error for $\delta^{18}O_{seawater}$ is about ± 0.16 ‰. We expect a similar error for $\delta^{18}O_{IVC\text{-}seawater}$ values.
144
145 **3. Results and Discussion**
146 *3.1 $SST_{Mg/Ca}$ in comparison with other lower-resolution temperature proxies from Site 610A*
147 Our high-resolution (3-4 kyr) *G. bulloides* $SST_{Mg/Ca}$ data of DSDP 610A cover the
148 time period ~4.0-3.3 Ma (Figs. 2a; 3). From ~4.0-3.7 Ma the $SST_{Mg/Ca}$ are ~16-18 °C which is
149 5-7 ºC warmer than the modern SSTs of ~11 ºC (Locarnini et al., 2010; see Fig. 1a). Gradual
150 cooling starts at ~3.7 Ma and from 3.65-3.5 Ma $SST_{Mg/Ca}$ rapidly cool by ~3.5 °C with minima
151 < 14 ºC. At 3.5-3.3 Ma, our $SST_{Mg/Ca}$ show short-term warming episodes, which remain 1-2
152 ºC lower than during the preceding period 4-3.7 Ma.
153 The lower-resolution U^k_{37}' and TEX_{86}-derived SST from the same site show a similar
154 gradual temperature decline since during the early Pliocene (Fig. 3; Naafs et al., in review).
155 Due to their lower temporal resolution, these records unfortunately do not yet capture the
156 abrupt cooling from 3.65-3.5 Ma we observe in $SST_{Mg/Ca}$ (Fig. 3).
157 Although all proxies indicate a similar relative temperature change, absolute U^k_{37}' and
158 TEX_{86}-derived SST are ~2-3 ºC warmer than our $SST_{Mg/Ca}$ (Fig. 3; Naafs et al., in review).
159 This temperature offset might be explained by changes in the Mg/Ca of the seawater through
160 time. A recent study suggested seawater Mg/Ca ratios during the Pliocene might have been
161 0.9 mol/mol lower than modern (Evans et al., 2016). Using this lower Mg/Ca seawater ratio
162 results in ~2 ºC higher $SST_{Mg/Ca}$ for the Pliocene. However, this study was based on *G. ruber*
163 and currently it does not exist a species-specific correction for *G. bulloides*, the species that
164 was used in our study. A multi-proxy SST study from the North Atlantic compared *G.*
165 *bulloides* $SST_{Mg/Ca}$ and alkenone-derived temperatures during the Mid-Pliocene (~ 3.0 Myr)
166 and found varying temperature offsets from -1 to 2 ºC depending on the latitude of the

selected core site (Robinson et al., 2008). These varying offsets cannot be related to the global changes in the Mg/Ca of seawater and their effect on $SST_{Mg/Ca.}$ In contrast, these offsets were explained by different habitat depths of the producing organisms, different growing seasons, different proxy SST calibrations and other chemical parameters (Robinson et al., 2008). For instance, *G. bulloides* lives in the upper 50-60 m water depth, while phototrophic coccolithophorids that produce alkenones thrive at clearly shallower depths (0-10 m; Müller et al., 1998; Kucera, 2009). The difference in habitat depths of the different organisms alone might explain a substantial part of the offset we observe. At present the annual water temperature gradient between 0 and 60 m water depth is about 0.8 ºC (Locarnini et al., 2010). This offset might have changed spatially due to the local oceanography as well as seasonally at Site 610A, (53ºN).

Independent of any effects of Mg/Ca of the seawater on our absolute $SST_{Mg/Ca}$ reconstructions, the relative $SST_{Mg/Ca}$ changes are similar as observed in the organic temperature proxies and considered robust. This is further justified because we here present a relatively short record of ~700 kyrs, shorter than the residence times of both Mg and Ca in seawater (Li, 1982).

3.2 Deciphering changes in the AMOC

Our observed prominent 3 °C cooling around 3.65-3.5 Ma is consistent with other Pliocene data from sites influenced by the NAC. Nearby Site 552A shows a similar magnitude of cooling of about 3-4 °C (Fig. 4a; Karas et al., 2017). Alkenone-derived SSTs from Site 642 in the Norwegian Sea within the northeastern extension of the NAC also record this cooling (Figs. 1, 4a; Bachem et al., 2018).

The pronounced cooling at ~3.65-3.5 Ma is accompanied by a marked freshening of surface waters, reflected by the decreasing $\delta^{18}O_{IVC\text{-}seawater}$ values by ~0.7‰ (smoothed record) (Fig. 4a, b). For the remainder of the record $\delta^{18}O_{IVC\text{-}seawater}$ values from Site 610A fluctuate,

showing at times fresher or more saline conditions, however staying on average ~0.5 ‰ fresher compared to the time period before 3.65 Ma. Within the glacial MIS M2 event they again show an abrupt freshening of approximately the same amplitude as during the 3.65-3.5 Ma period (data during M2 event is from De Schepper et al., 2013; Fig. 4b). This freshening and cooling around 3.65-3.5 Ma indicates an additional weakening of the NAC more than 300 ka prior to the NAC weakening during M2 (Fig. 4a, b; De Schepper et al., 2013). Note that for comparability the $\delta^{18}O_{IVC\text{-}seawater}$ values of the study of De Schepper et al. (2013) were re-calculated using the same method as used for our data.

Our notion that the observed sea surface cooling at Site 610A (and other sites in the region) responded mainly due to a reduction of the NAC during 3.65-3.5 Ma, not to global climate change is supported by the comparison with atmospheric CO_2 reconstructions and other SST records from the North Atlantic (Fig. 5). Atmospheric pCO_2 reconstructions from proxy data (Bartoli et al., 2011) and from a model simulation (Berends et al., 2019; based on the LR04 stack; Lisiecki and Raymo, 2005) show an increase at this time (Fig. 5b). Alkenone-derived SST from subtropical Site U1313 (Naafs et al., 2010) are in very good accordance with these increasing global atmospheric CO_2 indicating a slight warming trend (Fig. 5a,b). Even a pronounced warming of about 3 ºC is observed at the more northern Site 982 (Lawrence et al., 2009; Fig. 5a). This suggests that Site U1313 and at least partly Site 982 reacted to a slight global warming trend potentially related to an increase in pCO_2, whereas Site 610A (and 552A and 642 along the path of the eastern NAC) cooled due to a reduced NAC.

Our observed surface cooling and freshening trends of the NAC around ~3.65-3.5 Ma are accompanied by decreasing benthic foraminiferal $\delta^{13}C$ records from southern Atlantic Sites 1264 (2505 m water depth) and 1267 (4355 m water depth) by ~0.5 ‰ (Fig. 4a, b, c; Bell et al., 2014). The benthic $\delta^{13}C$ records of both sites were interpreted in terms of changes in NADW export towards the South Atlantic (Bell et al., 2014). That is because these sites are

219 at the limit between NADW from the North and deepwater masses from the South (Antarctic
220 Bottom Water at Site 1267; Bell et al., 2014; Farmer et al., 2019). Low $\delta^{13}C$ values of the
221 seawater (lower than 1‰) point to a higher contribution of Antarctic Bottom Waters and a
222 reduced presence of NADW in the South Atlantic, which source region is commonly
223 characterized by high $\delta^{13}C$ values (higher than 1 ‰; Kroopnick, 1985; Raymo et al., 1992;
224 Bell et al., 2014). Hence, the decreasing South Atlantic benthic $\delta^{13}C$ records point to the
225 overall reduced export of NADW into the South Atlantic during ~3.65-3.5 Ma, in line with a
226 weaker deep AMOC circulation (Fig. 4c; Bell et al., 2014). This interpretation is consistent
227 with the evidence of fresher conditions at Site 610A in response to the reduction in the NAC
228 as less saline waters in the northern North Atlantic would weaken deep water formation.
229
230 *3.3 Implications of the weakening of the AMOC for the iNHG*
231 The proposed NAC/AMOC weakening around ~3.65-3.5 Ma took place at the same
232 time as increased sea ice extent in the Arctic Ocean. Although low-resolution, sea ice
233 biomarker data (IP_{25} and $PIP2_5$) from ODP Site 910C off Spitsbergen reached the modern
234 minimum summer extent during this time (Fig. 4d; Knies et al., 2014a). Two ice rafted
235 detritus (IRD) maxima between 3.6-3.5 Ma and another one during the M2 event in nearby
236 Site 911A support the notion of sea ice expansion and strengthened Arctic glaciation at that
237 time (Fig. 4d; Knies et al., 2014b). These Arctic Ocean sites are within the West Spitsbergen
238 Current that today is the warm and saline direct extension of the Norwegian Current from the
239 South (Hanzlick, 1983; Knies et al., 2014b). As such this northernmost eastern extension of
240 the NAC into the cold Arctic (Hanzlick, 1983) should have sensitively reacted on our
241 observed changes in NAC/AMOC strength. That means the reduced heat and salt transport
242 along the NAC most likely facilitated the registered sea ice growth in this part of the Arctic
243 Ocean during a time of slightly warmer global temperatures. Extended sea ice cover in the
244 Arctic Ocean started as early as around 4.5 Ma, however it was restricted to the present area

245 of the cold and fresh East Greenland Current (EGC) Site 907 (See Figure 1 for location;
246 Clotten et al., 2019). The tectonic restriction of the Panama Seaway and the inflow of Pacific
247 Waters through the Bering Strait most likely initiated the cold and fresh EGC at this time (De
248 Schepper et al., 2015; Clotten et al., 2019).

249 NAC temperatures at Sites 610A, 552A and 642 (Karas et al., 2017; Bachem et al.,
250 2018) stay on average about 2-3 ºC colder after 3.6 Ma, than before, even during the mid-
251 Pliocene warmth interval (following the M2 event; Fig. 4a). This is inline with the extended
252 sea ice in the Arctic Ocean, which did not fully reverse during subsequent warmer intervals
253 after the M2 event (see Fig. 4d,e). We hence suggest that the NAC/AMOC induced extension
254 of arctic sea ice starting at 3.65 Ma might have been an important amplifier for Arctic climate
255 change and Northern Hemisphere continental glaciation (Mudelsee and Raymo, 2005).
256 Extended sea ice in the entire Arctic Ocean would have increased the albedo that would have
257 further cooled the region amplifying the growth of continental ice sheets. Pliocene tectonic
258 uplift of adjacent land areas might have supported this cooling process (Knies et al., 2014b
259 and refs. therein). Indeed, further evidence for increased sea ice formation around 3.65-3.5
260 Ma comes from the Barents Sea (De Schepper et al., 2014 and refs. therein) and continental
261 ice sheets formed on Greenland, Iceland, and in the mid-latitudes of the low lands of Canada
262 around this time (Goa et al., 2012; De Schepper et al., 2014 and references therein). Extensive
263 continental glaciations in both hemispheres, however, did not start until the M2 event at ~ 3.3
264 Ma (Fig. 4e; De Schepper et al., 2014 and refs. therein).

265 Our notion on a reduced NAC/AMOC amplifying high northern latitude sea ice
266 growth and continental glaciation at 3.65 Ma differ with other hypothesises (Driscoll and
267 Haug, 1998; Knies et al., 2014a; Clotten et al., 2019) who argue that increased northward
268 moisture transport via AMOC was the ultimate prerequisite for this climatic development.
269 Alternatively, we here argue that during 3.65-3.5 Ma this oceanic induced moisture transport
270 was not necessary for the build up of continental ice sheets and sea ice as the warm Pliocene

world already offered more precipitation than at modern (Salzmann et al., 2009). Hence, we here emphasize the importance of reduced heat and salt transport towards the high northern latitudes for the iNHG.

3.4 Why a weakening of the NAC/AMOC?

A weakening of the AMOC during the Pliocene was discussed previously. Frank et al. (2002) argued from low-resolution radiogenic isotopes from the North and South Atlantic for an AMOC slowdown during the last 4-3 Ma. Similarly, it was deduced from benthic $\delta^{13}C$ records from the Ceara Rise (sites 925 and 929) that the AMOC decelerated at times during 3.7-3.3 Ma (Billups et al., 1997). This AMOC weakening was initially related to the general cooling trend at the onset of iNHG. Alternatively, a recent study discussed the roles of the closing/opening of seaways, in particular the Indonesian Seaway and the Bering Strait on the observed weakening of the AMOC during 3.8-3 Ma (Karas et al., 2017). Whereas the opening of the Bering Strait is in principle a viable mechanism to weaken the AMOC, its Pliocene history is not well constrained (Karas et al., 2017; De Schepper et al., 2015 and refs. therein). Despite of speculations about re-opening/closing events during the Pliocene (Naafs et al., in review) such an occurrence during 3.65-3.5 Ma remains uncertain.

The considerable and effective constriction of the Indonesian Seaway is placed between 4-3 Ma (Cane and Molnar, 2001) with most distinct oceanographic effects around 3.55 Ma (Karas et al., 2009; Auer et al., 2019). This tectonic narrowing likely caused an enhanced transport of fresher waters via the Agulhas Current into the Atlantic Ocean that weakened the AMOC and affected sea surface conditions in the North and South Atlantic (Karas et al., 2017 and references therein). It hence appears reasonable to us that our observed rapid weakening of the NAC at 3.65-3.5 Ma was at least partly caused by this remote plate-tectonic process. In a positive feedback loop, the continuous freshening of the northern North

296 Atlantic would have then reduced the subduction of these surface waters, further impeding the
297 formation of NADW and weakening the AMOC.
298
299 **4. Conclusions**
300 We here present high-resolution records of *G. bulloides* $SST_{Mg/Ca}$, changes in surface salinities
301 (expressed as $\delta^{18}O_{IVC\text{-}Seawater}$) from North Atlantic Site 610A in the northern North Atlantic for
302 the period 4-3.3 Ma. Our data show a marked cooling (~3.5 °C) and freshening (~0.7‰) from
303 3.65-3.5 Ma. This time period is accompanied by a decrease in benthic $\delta^{13}C$ from South
304 Atlantic Ocean sites meaning a weaker NADW and AMOC strength (Bell et al., 2014). We
305 speculate that the weakened AMOC and colder and fresher surface waters in the North
306 Atlantic around 3.65 Ma allowed for sea ice extension in the Arctic Ocean that might have
307 preconditioned the climate for subsequent continental ice sheet growth.
308
309 **Acknowledgements**
310 We thank the IODP for providing the samples of this study. For technical support we thank J.
311 Fiebig, S. Hofmann and C. Neu (Frankfurt) and C. Evans (UoB). C.K. thanks the German
312 Research Foundation (DFG) for funding within project KA3461/1-2. BDAN is supported
313 through a University Research Fellowship, funded by the Royal Society and Tata Group.
314
315 **Data availability**
316 All data is available at the World Data Center for Paleoclimatology (WDC Paleo):
317 https://www.ncdc.noaa.gov/paleo/wdc-paleo.html.
318
319 **References**

Auer, G. et al., 2019. Timing and Pacing of Indonesian Throughflow Restriction and Its Connection to Late Pliocene Climate Shifts. Paleoceanography and Paleoclimatology, https://doi.org/10.1029/2018PA003512.

Bachem, P.E. et al., 2018. Highly variable Pliocene sea surface conditions in the Norwegian Sea. Clim. Past 13, 1153-1168. https://doi.org/10.5194/cp-13-1153-2017.

Barker, S., Greaves, M., Elderfield, H., 2003. A study of cleaning procedures used for foraminiferal Mg/Ca paleothermometry. Geochem., Geophys., Geosyst. 4 (9), 8407, doi:10.1029/2003GC000559.

Bartoli, G. et al., 2011. Atmospheric CO2 decline during the Pliocene intensification of Northern Hemisphere glaciations. Paleoceanography 26, PA4213, doi:10.1029/2010PA002055.

Bell, D.B. et al., 2014. Local and regional trends in Plio-Pleistocene δ18O records from benthic foraminifera. Geochem., Geophys., Geosyst. 15(8), 3304–3321.

Berends, C.J., et al., 2019. Modelling ice sheet evolution and atmospheric CO2 during the Late Pliocene. Clim. Past 15, 1603–1619.

Billups, K. et al., 1997. Early Pliocene deep-water circulation: Stable isotope evidence for enhanced northern component deep water. In: Shackleton, N.J., Curry, W.B., Richter, C., and Bralower, T.J. (Eds.) Proceedings of the Ocean Drilling Program, Scientific Results, 154.

Cane, M., Molnar, P., 2001. Closing of the Indonesian seaway as a precursor to east African aridification around 3–4 million years ago. Nature 411, 157–162.

Clotten, C. et al., 2019. On the causes of Arctic sea ice in the warm Early Pliocene. Scientific Reports 9, DOI:10.1038/s41598-018-37047-y.

de Boer, B. et al., 2014. Persistent 400,000-year variability of Antarctic ice volume and the carbon cycle is revealed throughout the Plio-Pleistocene. Nat. Comm. 5, 2999. doi: 10.1038/ncomms3999.

346 De Schepper, S. et al., 2013. Northern Hemisphere Glaciation during the Globally Warm
347 Early Late Pliocene. PLoS ONE 8(12): e81508. doi:10.1371/journal.pone.0081508.
348 De Schepper, S. et al., 2014. A global synthesis of the marine and terrestrial evidence for
349 glaciation during the Pliocene Epoch. Earth-Science Reviews 135, 83-102,
350 https://doi.org/10.1016/j.earscirev.2014.04.003.
351 De Schepper, S. et al., 2015. Early Pliocene onset of modern Nordic Seas circulation related
352 to ocean gateway changes. Nature Comm. 6, 8659.
353 de Villiers, S. et al., 2002. An intensity ratio calibration method for the accurate determination
354 of Mg/Ca and Sr/Ca of marine carbonates by ICP-AES. Geochem. Geophys. Geosyst. 3,
355 1001, doi:10.1029/2001GC000169.
356 Driscol, N.W., Haug, G.H., 1998. A short circuit in thermohaline circulation: A cause for
357 northern hemisphere glaciation? Science 282(5388), 436-438.
358 Elderfield, H., Ganssen, G., 2000. Past temperature and δ18O of surface ocean waters inferred
359 from foraminiferal Mg/Ca ratios. Nature 405, 442–445.
360 Evans, D. et al., 2016. Planktic foraminifera shell chemistry response to seawater chemistry:
361 Pliocene-Pleistocene seawater Mg/Ca, temperature and sea level change. Earth and Planet.
362 Sci. Lett. 438, 139-148.
363 Farmer, J.R. et al., 2019. Deep Atlantic Ocean carbon storage and the rise of 100,000-year
364 glacial cycles. Nature Geosciences 12, 355-360.
365 Frank, M. et al., 2002. North Atlantic Deep Water export to the Southern Ocean over the past
366 14 Myr: Evidence from Nd and Pb isotopes in ferromanganese crusts. Paleoceanography
367 17, 12-1 to 12-9.
368 Goa, C. et al., 2012. Glaciation of North America in the James Bay Lowland, Canada,
369 3.5 Ma. Geology 40, 975-978.

370 Greaves, M. et al., 2008. Interlaboratory comparison study of calibration standards for
371 foraminiferal Mg/Ca thermometrie. Geochem. Geophys. Geosyst. 9, Q08010,
372 doi:10.1029/2008GC001974.
373 Hanzlick, D.J., 1983. The west Spitsbergen current: transport, forcing, and variability. PHD
374 thesis, University of Washington, 145pp.
375 https://apps.dtic.mil/dtic/tr/fulltext/u2/a137532.pdf.
376 Haug, G.H., Tiedemann, R., 1998. Effect of the formation of the Isthmus of Panama on
377 Atlantic ocean thermohaline circulation. Nature 393, 673–676.
378 Hut, G., 1987. Consultants' group meeting on stable isotope reference samples for
379 geochemical and hydrological investigations. Rep. to Dir. Gen., Int. Atomic Energy,
380 Agency, Vienna.
381 Jackson, L.C. et al., 2015. Global and European climate impacts of a slowdown of the AMOC
382 in a high resolution GCM. Clim. Dyn. 45, 3299-3316.
383 Jonkers, L. et al., 2013. Seasonal patterns of shell flux, d18O and d13C of small and large N.
384 pachyderma (s) and G. bulloides in the subpolar North Atlantic. Paleoceanography 28(1),
385 164-174
386 Karas, C. et al., 2009. Mid-Pliocene climate change amplified by a switch in Indonesian
387 subsurface throughflow. Nature Geoscience 2, 434–438, doi: 10.1038/NGEO520.
388 Karas, C. et al., 2017. Pliocene oceanic saways and global climate. Scientific Reports 7,
389 39842.
390 Knies, J. et al., 2014a. The emergence of modern sea ice cover in the Arctic Ocean. Nat.
391 Comm. 5, https://doi.org/10.1038/ncomms6608.
392 Knies, J. et al., 2014b. Effect of early Pliocene uplift on late Pliocene cooling in the Arctic–
393 Atlantic gateway. Earth Planet Sci Lett. 387, 132-144.
394 Kroopnick, P., 1985. The distribution of carbon-13 in the world oceans. Deep Sea Res. 32,
395 57-84.

Kucera, M., 2009. Determination of Past Sea Surface Temperatures, in J.H. Steele (Ed.), Encyclopedia of Ocean Sciences (Second Edition), Academic Press, pp. 98-113. https://doi.org/10.1016/B978-012374473-9.00700-1.

Lawrence, K.T. et al., 2009. High-amplitude variations in North Atlantic sea surface temperature during the early Pliocene warm period. Paleoceanogr. Paleoclimatol. 24, PA2218, doi:10.1029/2008PA001669.

Li, Y.-H., 1982. A brief discussion on the mean oceanic residence time of elements. Geochim. Cosmochim. Acta 46, 2671–2675.

Lisiecki, L.E., Raymo, M.E., 2005. A Pliocene-Pleistocene stack of 57 globally distributed benthic d18O records. Paleoceanography 20, 1 PA1003, doi:10.1029/2004PA001071.

Locarnini, R.A. et al., 2010. World Ocean Atlas 2009, Volume 1: Temperature. S. Levitus, Ed. NOAA Atlas NESDIS 68, US. Government Printing Office, Washington, D.C., 184 pp.

Lunt, D.J. et al., 2008. Late Pliocene Greenland glaciation controlled by a decline in atmospheric CO2 levels. Nature 454, 1102-1106.

Mudelsee, M., Raymo, M.E., 2005. Slow dynamics of the northern hemisphere glaciation. Paleoceanography 20, PA4022, doi:10.1029/2005PA001153.

Müller, P.J. et al., 1998. Calibration of the alkenone paleotemperature index U37K′ based on core-tops from the eastern South Atlantic and the global ocean (60°N-60°S). Geochim. Cosmochim. Acta 62, 1757-1772.

Naafs, B.D.A. et al., 2010. Late Pliocene changes in the North Atlantic Current. Earth and Planet. Sci. Letters 298(3-4), 434-442, https://doi.org/10.1016/j.epsl.2010.08.023.

Naafs, B.D.A. et al., in revision for Paleoceanogr. Paleoclimatol. Repeated collapse of the Pliocene sea surface temperature gradient in the North Atlantic.

Raymo, M.E., Hodell, D., Jansen, E., 1992. Response of deep ocean circulation to initiation of Northern Hemisphere Glaciation (3-2 Ma). Paleoceanography 7, 645-672.

Robinson, M.M. et al., 2008. Reevaluation of mid-Pliocene North Atlantic sea surface temperatures. Paleoceanography 23, PA3213, doi:10.1029/2008PA001608.

Salzmann, U., Haywood, A.M., Lunt, D.J., 2009. The past is a guide to the future? Comparing Middle Pliocene vegetation with predicted biome distributions for the twenty-first century. Phil. Trans. R. Soc. A 367, 189-204.

Schiebel, R., Bijma, J., Hemleben, C., 1997. Population dynamics of the planktic foraminifer Globigerina bulloides from the eastern North Atlantic, Deep Sea Res., Part I, 44, 1701 – 1713, doi:10.1016/S0967-0637(97) 00036-8.

Schlitzer, R., 2012. Ocean Data View, http://odv.awi.de.

Shackleton, N. J., 1974. Attainment of isotope equilibrium between ocean water and the benthonic foraminiferal genus Uvigerina. Isotopic changes in the ocean during the last glacial. Cent. Nat. Rech. Sci. Colloq. Int. 219, 203.

Steph, S. et al., 2010. Early Pliocene increase in thermohaline overturning: A precondition for the development of the modern equatorial Pacific cold tongue. Paleoceanography 25, PA2202.

Trenberth, K.E., Fasullo, J.T., 2017. Atlantic meridional heat transports computed from balancing Earth's energy locally. Geophys. Res. Lett. 44, 1919–1927, doi:10.1002/2016GL072475.

Figure captions

Figure 1: North Atlantic surface and Atlantic deep ocean circulation. A) SST at 30 m water depth (color shading; Locarnini et al., 2010; Schlitzer, R. Ocean Data View, http://odv.awi.de, 2012). DSDP Site 610A (data of this study; red dot) and other sites for comparison are indicated (white dots). The warm North Atlantic Current (NAC) that feeds the

Norwegian Current and the cold East Greenland Current (EGC) are schematically indicated by white arrows. B) Simplified circulation patterns of the NADW (black lines). Deep water formation areas are indicated as white shaded areas. Circulation pattern is drawn according to Bell et al. (2014; and refs therein). Locations of other sites along the pathway of NADW discussed in the text are indicated (white dots). Site U1313 is indicated by a small circle.

Figure 2: Calculation of $\delta^{18}O_{seawater}$ and $\delta^{18}O_{IVC\text{-}seawater}$. (A) *G. bulloides* $\delta^{18}O$ (light blue) and $SST_{Mg/Ca}$ values (red) of Site 610A. (B) $\delta^{18}O_{seawater}$ values (brown) are calculated from combined *G. bulloides* $\delta^{18}O$ and $SST_{Mg/Ca}$ (error ±0.16 ‰). (C) Ice volume corrected $\delta^{18}O_{seawater}$ ($\delta^{18}O_{IVC\text{-}seawater}$; blue) reflecting relative changes in salinities. For the estimation of the global ice volume change during the Pliocene, we used (D), which is a simulated global ice volume $\delta^{18}O_{seawater}$ record ($\delta^{18}O_{GIV\text{-}seawater}$; de Boer et al., 2014; black). The error bars for $\delta^{18}O_{seawater}$ and $\delta^{18}O_{IVC\text{-}seawater}$ values are indicated (see methods). Smoothed thick lines in (B) and (C) are calculated based on a Stineman function with ±10% data range (performed with Kaleidagraph 4.1).

Figure 3: Comparison of $SST_{Mg/Ca}$, alkenone-derived SST and TEX_{86}-derived SST from Site 610A. $SST_{Mg/Ca}$ are from this study (red). Alkenone-derived SST (blue) and TEX_{86}-derived SST (stippled line) are from Naafs et al. (in revision). Error bars are indicated next to labels (see methods and Naafs et al., in revision).

Figure 4: Pliocene paleoceanographic data from the North Atlantic and other ocean areas. (A) *G. bulloides* $SST_{Mg/Ca}$ from North Atlantic Site 610A (red; this study) and during M2 (short record in purple; De Schepper et al., 2013) in comparison to *G. bulloides* $SST_{Mg/Ca}$ from Site 552A (light blue; Karas et al., 2017), alkenone-derived SST from Norwegian Sea Site 642 (dashed; Bachem et al., 2018). (B) $\delta^{18}O_{IVC\text{-}seawater}$ records from Site 610A (blue; this study) and from a previous study during glacial M2 event (green; De Schepper et al., 2013).

475 (C) Benthic $\delta^{13}C$ records from eastern South Atlantic sites 1264 (stippled line) and 1267 (red;
476 both from Bell et al., 2014), reflecting changes in NADW strength. (D) IP_{25} (purple) and PIP_{25}
477 (stippled line) from Site 910C as proxies for sea ice extent (Knies et al., 2014a). IRD events
478 are indicated based on the IRD record from Site 911A (Knies et al., 2014b). E) Simulated sea
479 level record over the Pliocene (deBoer et al., 2014). Smoothed lines in (B) and (E) are
480 calculated based on a Stineman function with ±10% data range (performed with Kaleidagraph
481 4.1). Error bars are indicated. Shaded area indicates the time period of substantial temperature
482 and salinity change from 3.65 Ma to 3.5 Ma 3.65-3.5 Ma at the beginning of the
483 intensification of Northern Hemisphere Glaciation (3.6-2.4 Ma; Mudelsee and Raymo, 2005).
484
485 **Figure 5: Site 610A $SST_{Mg/Ca}$, global climate, and other North Atlantic SST records.** (A)
486 Site 610A $SST_{Mg/Ca}$ (red; this study), alkenone-derived SST from Site U1313 (light blue;
487 Naafs et al., 2010), alkenone-derived SST from Site 982 (black; Lawrence et al., 2009). (B)
488 atmospheric CO_2 reconstructions from foraminiferal boron isotopes (blue; Bartoli et al., 2011)
489 and from a model simulation (black; Berends et al., 2019). Time period 3.65-3-5 Ma is
490 indicated as shaded area.
491

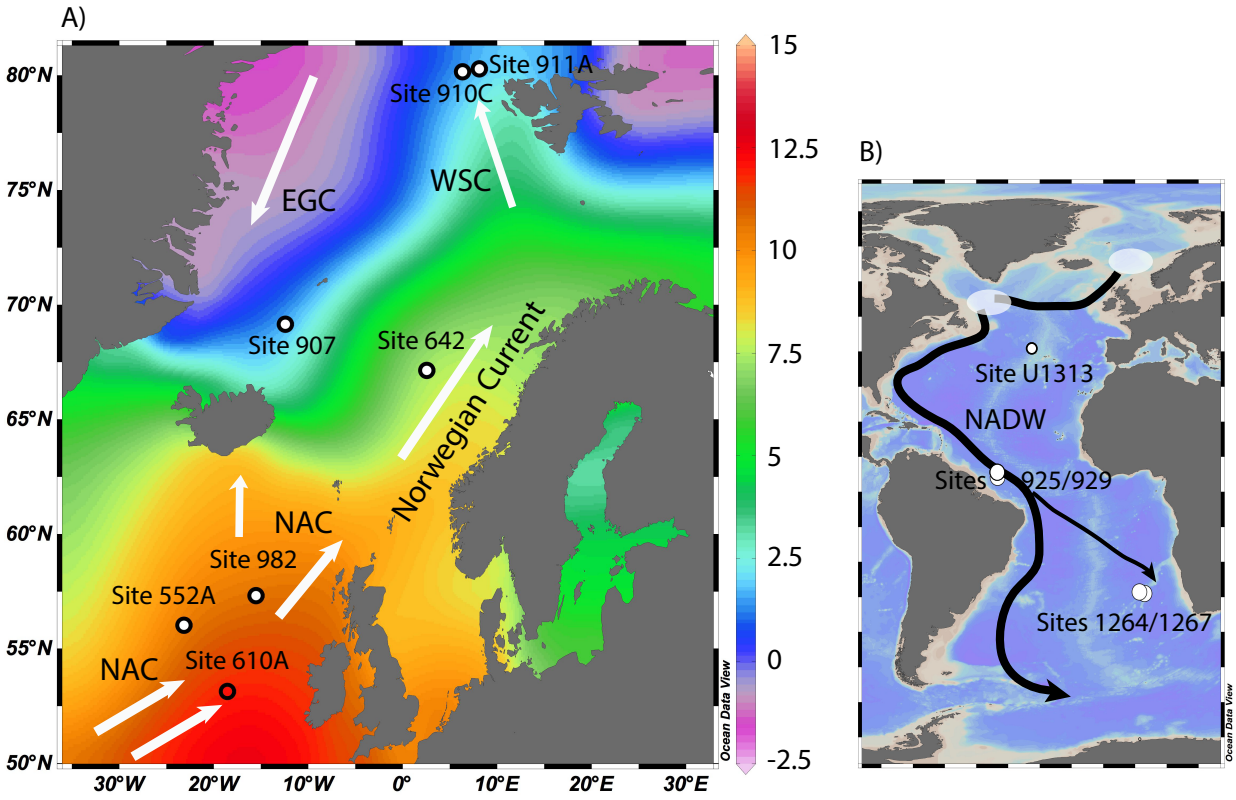
A)
Site 911A
Site 910C
EGC
WSC
Site 907
Site 642
Norwegian Current
NAC
Site 982
Site 552A
NAC
Site 610A
80°N
75°N
70°N
65°N
60°N
55°N
50°N
30°W
20°W
10°W
0°
10°E
20°E
30°E
15
12.5
10
7.5
5
2.5
0
-2.5
Ocean Data View
B)
Site U1313
NADW
Sites 925/929
Sites 1264/1267
Ocean Data View

Figure 1

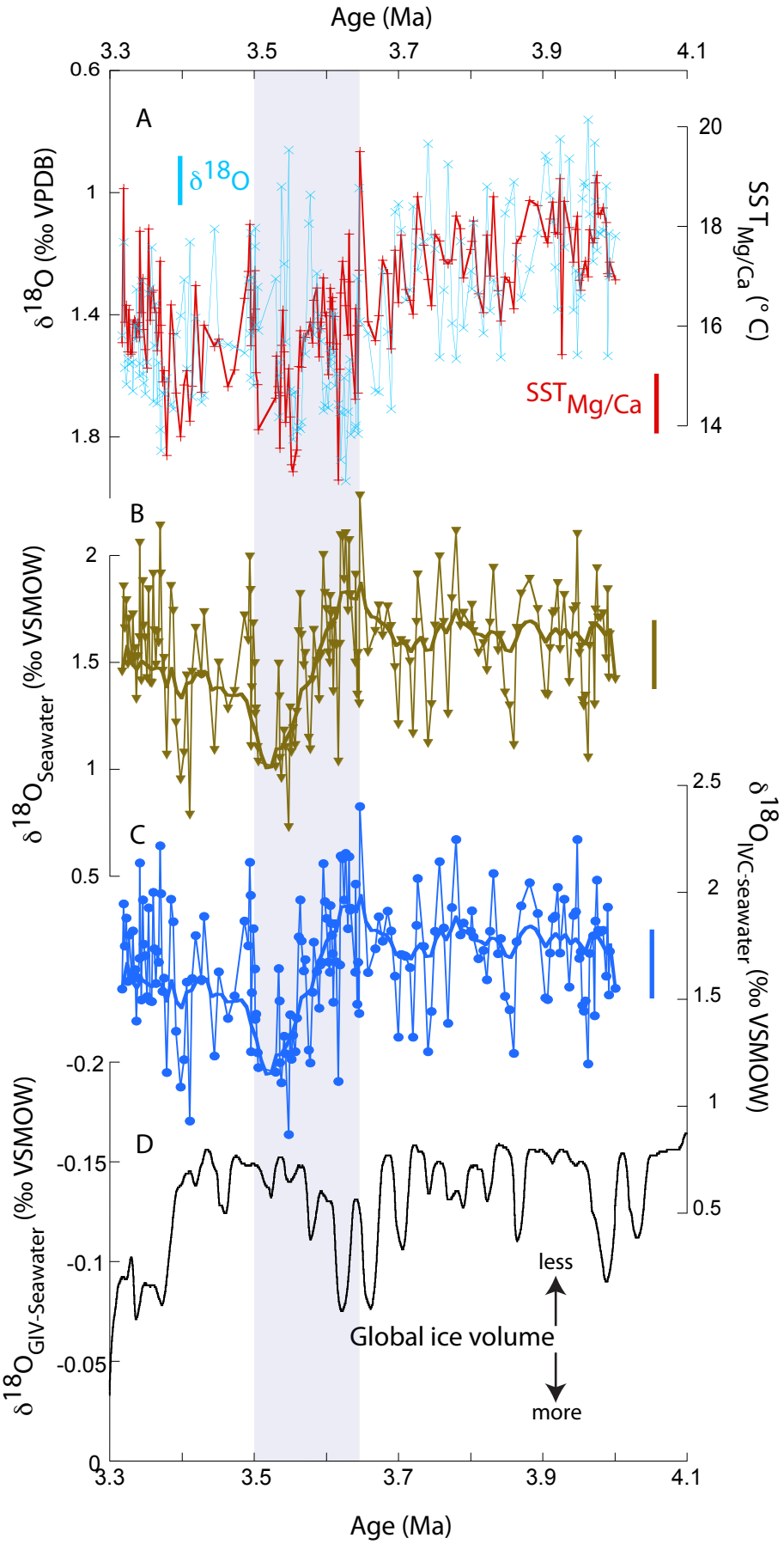
Age (Ma)
3.3
3.5
3.7
3.9
4.1
A
δ18O
SSTMg/Ca
δ18O (‰ VPDB)
SSTMg/Ca (° C)
0.6
1
1.4
1.8
20
18
16
14
B
δ18OSeawater (‰ VSMOW)
2
1.5
1
C
δ18OIVC-seawater (‰ VSMOW)
0.5
-0.2
2.5
2
1.5
1
0.5
D
δ18OGIV-Seawater (‰ VSMOW)
-0.15
-0.1
-0.05
0
less
Global ice volume
more
Age (Ma)

Figure 2

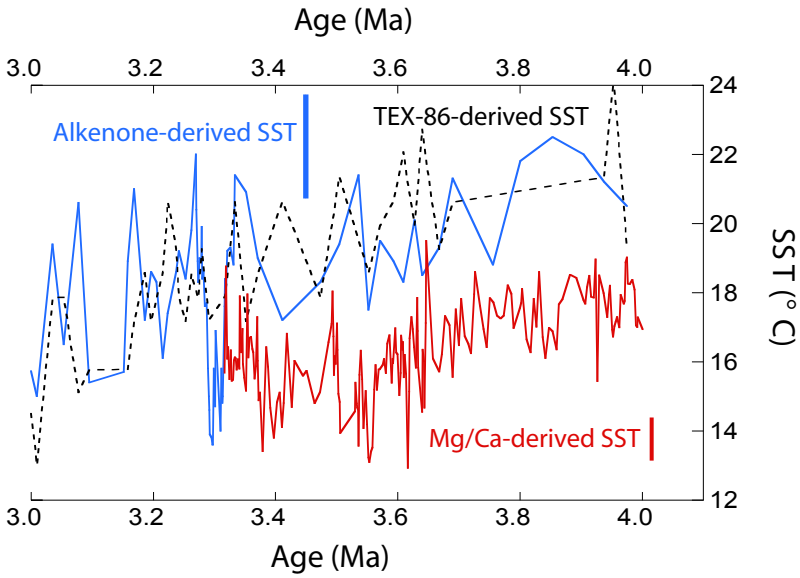
Age (Ma)
3.0
3.2
3.4
3.6
3.8
4.0
Alkenone-derived SST
TEX-86-derived SST
Mg/Ca-derived SST
24
22
20
18
16
14
12
SST (° C)
Age (Ma)

Figure 3

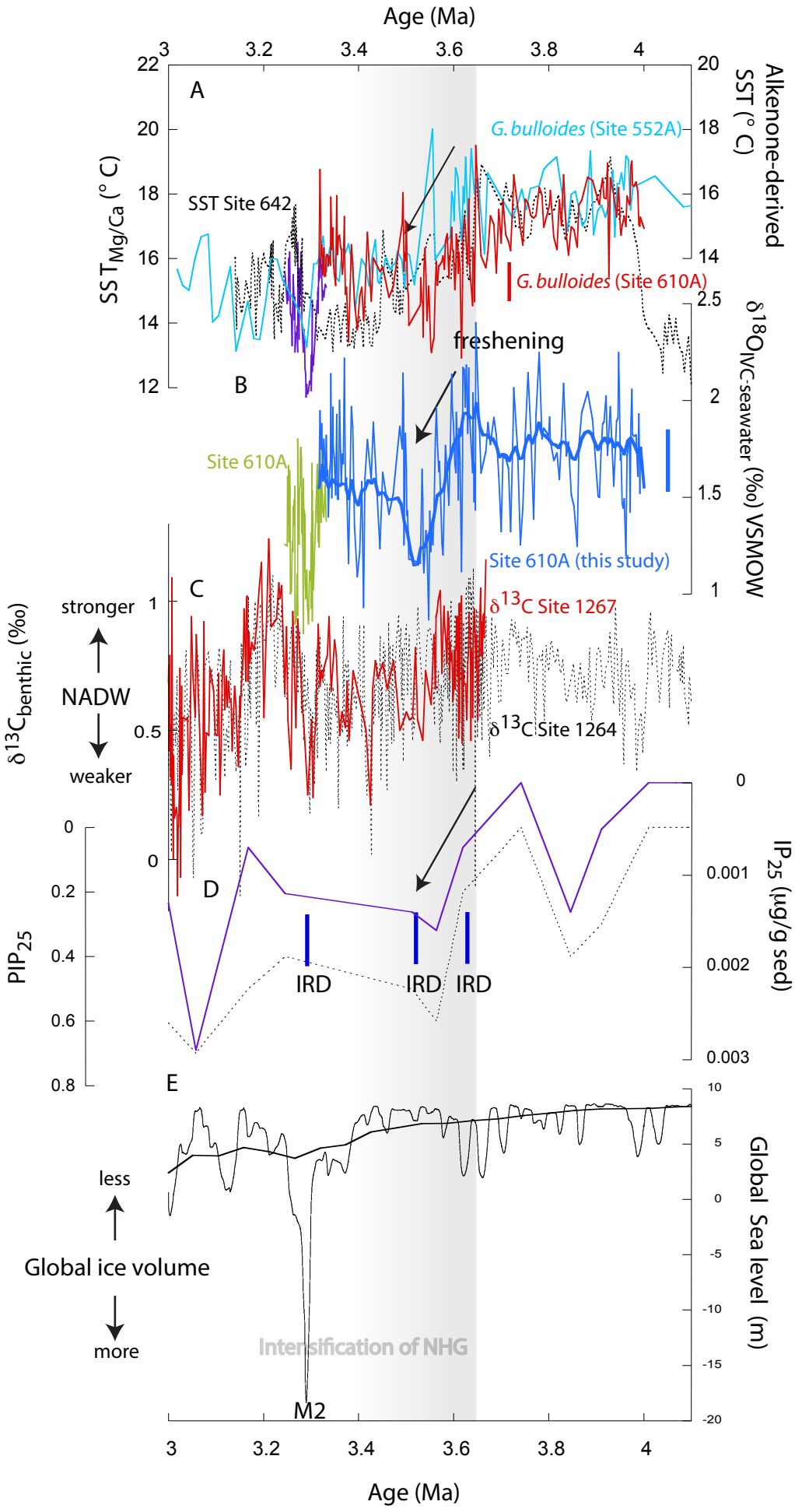
Age (Ma)
A
SST Site 642
G. bulloides (Site 552A)
G. bulloides (Site 610A)
SST $T_{Mg/Ca}$ (° C)
Alkenone-derived SST (° C)
B
freshening
Site 610A
Site 610A (this study)
$\delta^{18}O_{IVC\text{-}seawater}$ (‰) VSMOW
C
stronger
NADW
weaker
$\delta^{13}C_{benthic}$ (‰)
$\delta^{13}C$ Site 1267
$\delta^{13}C$ Site 1264
D
IRD
IRD
IRD
PIP_{25}
IP_{25} (µg/g sed)
E
less
Global ice volume
more
Intensification of NHG
M2
Global Sea level (m)
Age (Ma)

Figure 4

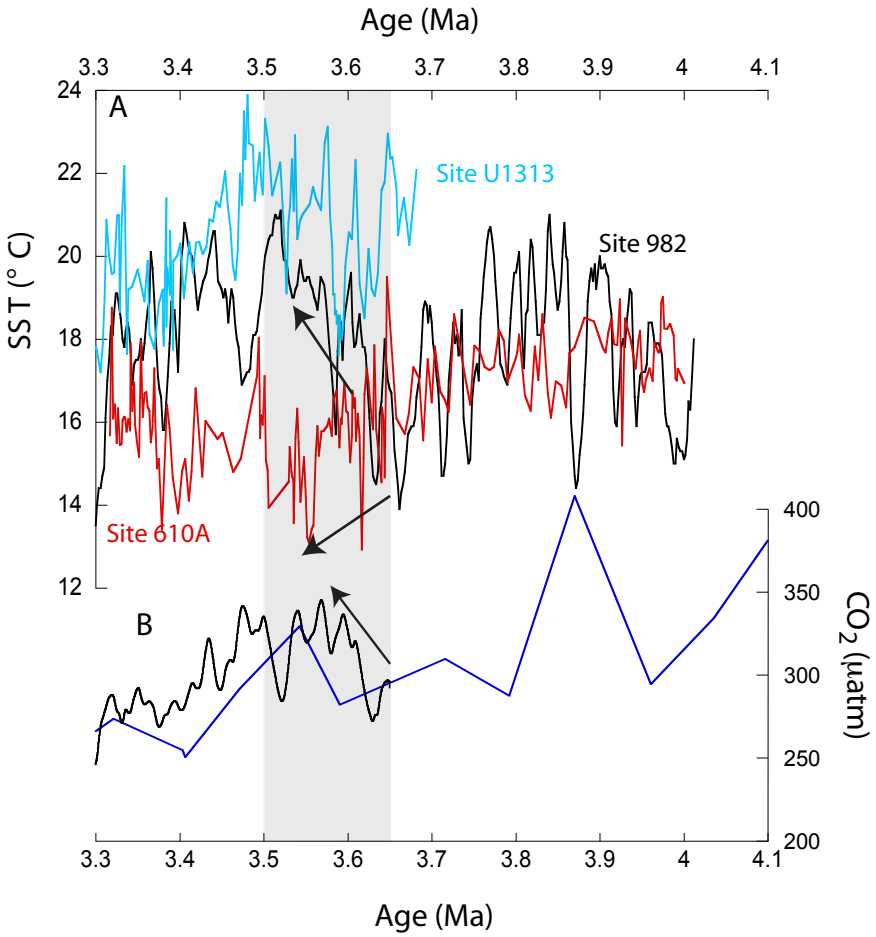
Age (Ma)
3.3
3.4
3.5
3.6
3.7
3.8
3.9
4
4.1
A
Site U1313
Site 982
Site 610A
SST (° C)
24
22
20
18
16
14
12
B
400
350
300
250
200
CO2 (µatm)
Age (Ma)

Figure 5